analytical chemistry

Article

pubs.acs.org/ac

Miniaturized Linear Wire Ion Trap Mass Analyzer

Qinghao Wu,[†] Ailin Li,[†] Yuan Tian,[†] Richard N. Zare,[‡] and Daniel E. Austin*[,†]

[†]Department of Chemistry and Biochemistry, Brigham Young University, Provo, Utah 84602, United States

[‡]Department of Chemistry, Stanford University, Stanford, California 94305-5080, United States

Supporting Information

ABSTRACT: We report a linear ion trap (LIT) in which the electric field is formed by fine wires held under tension and accurately positioned using holes drilled in two end plates made of plastic. The coordinates of the hole positions were optimized in simulation. The stability diagram and mass spectra using boundary ejection were compared between simulation and experiment and good agreement was found. The mass spectra from experiments show peak widths (fwhm) in units of mass-to-charge of around 0.38 Th using a scan rate of 3830 Th/s. The limits of detection are 137 ppbv and 401 ppbv for benzene and toluene, respectively. Different sizes of the wire ion trap can be easily fabricated by drilling holes in scaled positions. Other distinguishing features, such as high ion and photon transmission, low capacitance, high tolerance to mechanical and assembly error, and low weight, are discussed.

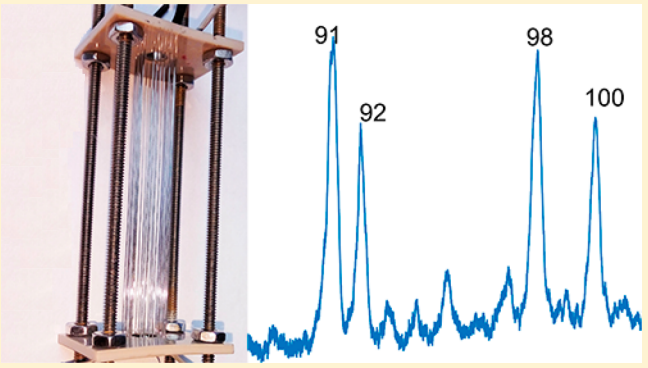

Mass spectrometry plays important roles in modern analytical chemistry due to high speed, high specificity, excellent sensitivity, and high resolving power.[1−5] However, the mass spectrometer has disadvantages of relatively large size, weight, power consumption, and complexity of maintenance. Some applications, such as public safety, environmental protection, and industrial process monitoring, require compact and portable instruments with good performance.[6−11] Quadrupole ion traps are among the best mass analyzers for miniaturization because of their compact size, relatively high working pressure, and the unique capability to perform multistage tandem mass analysis (MS^n).[12] The linear ion trap (LIT) has attracted recent attention due to higher ion transmission efficiency from an external ion source, increased ion storage volume, and good resolving power.[13] The conventional LIT, with hyperbolic-shaped electrodes, represents the benchmark for current ion trap performance.[13] However, the fabrication of the electrodes requires high accuracy and a sophisticated process, thus increasing the cost. The miniaturization of such an LIT is more complicated. Therefore, several efforts have been made to achieve good performance with simplified electrodes.

One such effort is the rectilinear ion trap (RIT), introduced in 2004 by Cooks and co-workers.[14] The RIT is composed of six flat, rectangular electrodes and features a large charge capacity and high trapping efficiency. The miniaturized RIT has good analytical performance and has been assembled in hand-held mass spectrometers.[15−18] On the basis of the geometry of an RIT, a polymer-based RIT was also developed.[19] The polymer-based RIT was shown to be light, less expensive, and to demonstrate the same performance as traditional machined devices of the same size. LIT versions with other variants of electrode shape, such as triangular,[20,21] half-round rod,[22] mesh,[23] asymmetrical arc,[24] and a combination of rectangular electrodes and half-round rod electrodes,[25] have also been reported. Our lab has studied the two-plate planar LIT and achieved good performance.[26,27] All these studies aimed to fabricate a portable mass analyzer while minimizing the deleterious effects on performance that typically accompany nonhyperbolic electrode shapes.

In most radial ejection LITs, the trapping electric field is generated by solid metal electrodes with machined slits for ion ejection. These slits can block a portion of the ejected ions, reducing the sensitivity. In the present study, we replace the electrode-slit design by producing the trapping field using a series of fine metal wires. These wires are held under tension and accurately positioned using four sets of holes machined in each of two plastic end-plates. We found that this geometry can provide good resolution if the electric field is properly designed. The term "wire ion trap" has been used by Ray et al. for a trap in atomic physics experiments.[28] The trap is formed by four square-shaped loops, separated in space, and held together by four stainless steel rods. In a Ph.D. thesis, a wire trap for quantum computing experiments was proposed.[29] The trap was formed by three wires (representing the top) and three wires at the bottom, perpendicularly crossing each other. In an earlier study, Wang et al. proposed a cone-shaped Paul ion trap that was formed by an umbrella framework of resistance wires or a helically wound resistance wire.[30] The electric fields in a quadrupole ion filter formed by wires have been described in

Received: May 10, 2016
Accepted: July 2, 2016
Published: July 2, 2016

DOI: 10.1021/acs.analchem.6b01830
Anal. Chem. 2016, 88, 7800−7806

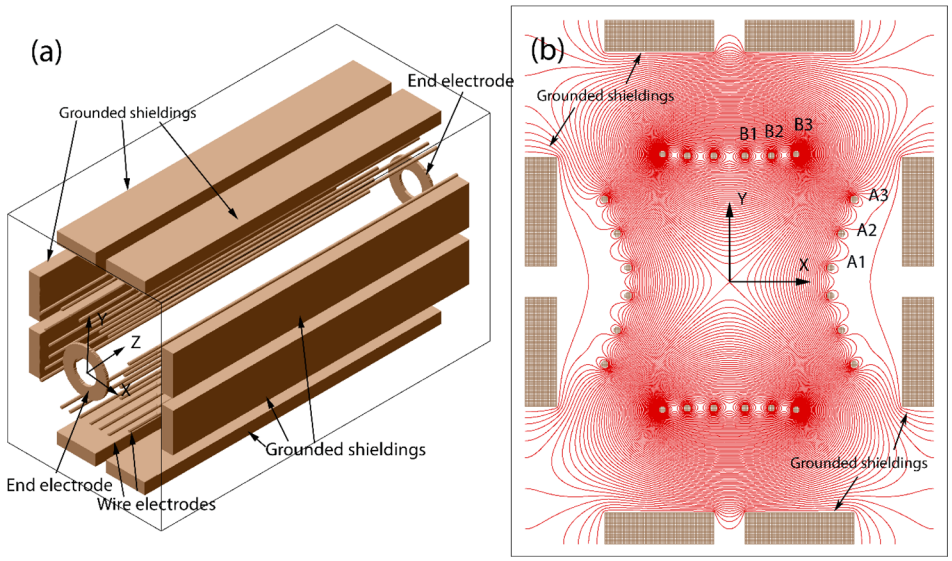

Figure 1. (a) LWIT model built in SIMION. (b) Calculated isopotential curves in the LWIT. A static potential (100 V) was applied on wires in the *Y* direction; all other electrodes are grounded.

U.S. Patents US 3501631 and US 4328420. These designs are different from the present device.

Because electric field optimization is essential to the design of any ion trap, much effort has been made to optimize the electric field by changing various geometrical parameters.[31,32] Simulations provide a way to test design changes with minimal investment in labor and cost. Two approaches are commonly used to predict trap performance. The first is calculating the higher-order components of electric field and comparing to values of existing traps.[33,34] However, because of arbitrary parameters, such as the boundary of the electric field and the degrees in polynomial curve fitting, this approach is not ideal as a general method for optimizing the geometry. The other approach is to estimate performance (e.g., mass resolution, ejection efficiency) using simulations. This provides a direct way to evaluate the geometry and can serve as a general way to optimize the geometry. The drawback of this method is that it requires intensive computation. With the progress of computation technology, this obstacle has been overcome to some extent.[35,36] In previous work,[37] we demonstrated a method of studying the misalignments in a two-plate LIT using a single-parameter optimization method, only one geometric parameter was varied and optimized at a time. However, the electrode geometry of ion traps can always be varied in multiple ways, in which case multiparameter optimization is desirable.

In this paper, we use a simulation method of optimizing multiple parameters based on the criterion of resolution and peak height to optimize six parameters in the Linear Wire Ion Trap (LWIT). A test system was built according to the optimized geometry. The stability diagram, resolution, and sensitivity of the LWIT were evaluated experimentally. In what follows we discuss the advantages of such a geometry, such as high ion transmission efficiency, good resolution, low capacitance, high tolerance to mechanical and assembly error, and low weight.

WIRE ION TRAP DESIGN

Design Overview. Figure 1a shows the model built for the wire ion trap. The rf potential was applied to the 12 wires in the *Y* direction (six in each direction). A potential of 23 V dc was applied to the two end electrodes to confine the ions in the *Z* direction. Grounded shields were used to shield the trap from the high negative potential of the detector. Simulation results show that the ion transmission efficiency through the slit is 0.78. These shielding electrodes could be replaced by metal grids to achieve a better ion transmission rate.

Figure 1b shows the isopotential curves for the LWIT. The isopotential curves in the center of the LWIT are very similar to that in a conventional hyperbolic LIT (Supporting Information Figure S1). However, in the LWIT, there are additional regions between the wires and grounded shields. The trapping/grounding fields penetrate through the wires, a situation that does not occur in solid-electrode traps. As a result, the grounded shielding has some effect on the fields but only in the proximity of the wires. Simulations show that the spacing between the wire array and the grounded shielding has an effect on ejection direction but not on mass resolution (Supporting Information Figure S2). Because the electric field and geometry are different from prior linear ion traps, a new method of optimization is needed.

Geometry Optimization. In the LWIT, the electric field in the center is primarily determined by the positions of 24 wires and the ground electrodes. Because of the symmetry in *XY* plane, there are a total of six independent wires, as labeled in Figure 1b. Because each independent wire has two position parameters (coordinates in *X* and *Y*), there are 12 independent variables, making geometry optimization challenging. To further reduce the parameters, we fixed the *X* coordinates for the top wires (B1, B2, and B3) and fixed the *Y* coordinates for the side wires (A1, A2, and A3) so that they are evenly spaced in those directions. In this way, the number of independent parameters is reduced to six.

We developed a user program in SIMION 8.1 (Scientific Instrument Services, Inc., Ringoes, NJ) that simulates mass spectra for a set of two-parameter combinations of geometries for two wires. For example, to optimize the *Y* positions of B1 and B2, the user program generates a mass spectrum for each geometry. The mass resolutions and peak heights are extracted from the simulated mass spectra using Matlab (Mathworks, Natick, MA).

DOI: 10.1021/acs.analchem.6b01830
Anal. Chem. 2016, 88, 7800−7806

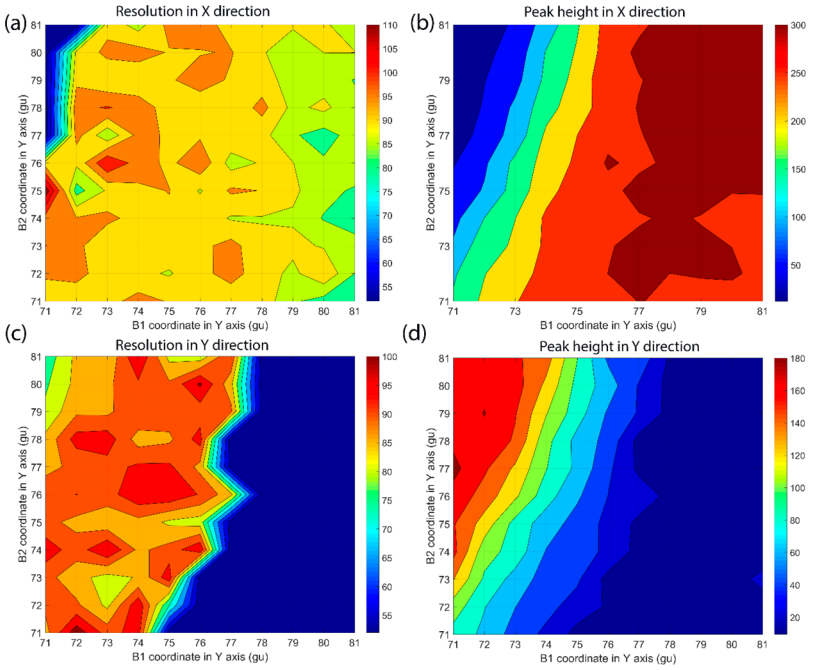

Figure 2. Optimization results for positions of B1 and B2. (a) The mass resolution abstracted from mass spectra obtained in the *X* direction. (b) The peak height abstracted from mass spectra obtained in the *X* direction. (c) The mass resolution abstracted from mass spectra obtained in the *Y* direction. (d) The peak height abstracted from mass spectra obtained in the *Y* direction. The unit for the coordinate is SIMION grid unit (gu). The color bars in parts a and c represent the resolution, and the color bars in parts b and d represent the peak intensity. Discontinuities in parts a and c compared to parts b and d arise from statistical fluctuations in the relatively small number of detected ions.

Table 1. Mass Range in Different Size Scales and *q* Values with rf Amplitude from 200 to 1000 $V_{0\text{-}p}$ and rf Frequency at 1.5 MHz

		$\omega = (1/2)\Omega$, $q = 0.908$		$\omega = (1/3)\Omega$, $q = 0.78$		$\omega = (1/5)\Omega$, $q = 0.283$	
dimensions, height × width	LWIT scale (mm per grid)	mass range from	mass range to	mass range from	mass range to	mass range from	mass range to
15.2 mm × 13.4 mm	0.1	11	54	12.5	67	35	191
7.6 mm × 6.7 mm	0.05	43	216	49	270	140	763
3.04 mm × 2.68 mm	0.02	275	1350	312.5	1675	875	4775
1.52 mm × 1.34 mm	0.01	1100	5400	1250	6700	3500	19100

This simulation strategy is derived from our previous work.[37] In the present study, a model of the LWIT was set up with a scale of 0.05 mm per grid unit. All mass spectra were obtained under the parameters of initial trapping amplitude of 380 V (0-p), radio frequency (rf) at 1.53 MHz, time step of 20 ns, and 3000 ions with mass-to-charge ratio of 91 Th. Other parameters in the user program and the mass spectra analysis method are same as published previously.[37]

As the ions could be ejected in both the *X* and *Y* directions, the mass spectra were collected from both directions. Figure 2 shows the mass resolution and peak height collected in both directions under all the geometries in B1 (from 71 to 81 gu in the *Y* axis) and B2 (from 71 to 81 gu in the *Y* axis). To avoid inaccurate results, mass spectra with fewer than 200 detected ions were discarded and are shown as the blue areas in Figure 2a,c.

Figure 2 indicates useful information on optimizing the B1 and B2 coordinates in the *Y* direction. First of all, ions are likely ejected in the *X* direction rather than in the *Y* direction. The maximum peak height from mass spectra in the *X* direction (Figure 2b) is much stronger than that from mass spectra in the *Y* direction (Figure 2d). Second, the resolution is not very sensitive to the wire positions. The mass resolution in Figure 2a ranges from 90 to 105 when B1 ranges from 73 to 78 and B2 ranges from 71 to 81. Considering the error in the resolution calculation, this range is relatively small. These results indicate that the coordinates of the wires could be positioned with low accuracy (±2 gu, ±0.1 mm) without a significant reduction in the resolution. Third, the B1 coordinate significantly affects the peak height. Increasing the B1 coordinate increases the peak height in the mass spectrum in the *X* direction but reduces the peak height in the *Y* direction.

To balance the peak intensity and resolution, we selected B1 = 76 and B2 = 76 as the best geometry. The other four parameters from relative wires were also optimized in this way. This method is based on the assumption that a global maximum exists in the optimizing process. Otherwise, the optimized geometry is a local maximum. The final coordinates for the six independent wires are A1 (67, 9), A2 (71, 31), A3 (80, 53), B1 (10, 76), B2 (27, 76), and B3 (43, 77).

EXPERIMENTAL SECTION

Size Scale of LWIT. The scale of the LWIT can be easily changed by drilling holes in different positions. The mass range was studied under a fixed rf amplitude scan range (from 200 to 1000 $V_{0\text{-}p}$) and a fixed frequency (1.5 MHz). Mass ranges at q = 0.78, q = 0.283, and q = 0.908 are calculated from simulation results. Table 1 shows simulation results on the mass range for ions ejected for different q values and different dimensional scales. The trap height is defined as the distance between the

DOI: 10.1021/acs.analchem.6b01830
Anal. Chem. 2016, 88, 7800−7806

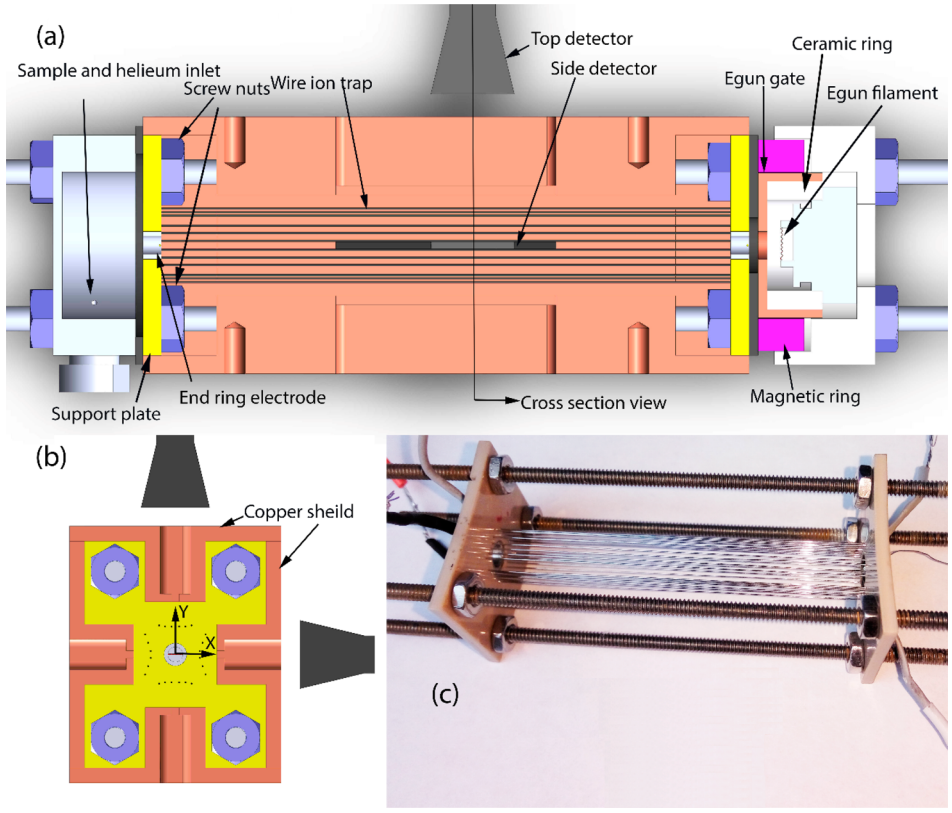

Figure 3. (a) Side view of designed LWIT test system. (b) Cut view of LWIT test system. (c) Assembled LWIT without the supporting metal shield and ion source.

top wire and bottom wire that are closest to the center (Figure 1b). Similarly, the width is defined as the distance between the left wire and right wire that are closest to the center. Note that the height and width are different from x_0 and y_0 in the conventional hyperbolic linear ion trap due to the lack of a continuous electrode surface in the present device. We treat the scale at 0.1 mm per grid as the full-size LWIT ($H \times W$ = 15.2 mm × 13.4 mm) and 0.05 mm per grid as half-size LWIT ($H \times W$ = 7.6 mm × 6.7 mm). Our current rf power supply has an amplitude range from 200 to 800 V 0-p at 1.53 MHz. Therefore, the geometry scale at half-size was selected for instrument construction due to the reasonable mass range that can be obtained with our current rf power supply.

LWIT Test System. The configuration of the LWIT test system is shown in Figure 3a, and a cross section is shown in Figure 3b. Figure 3c shows the assembled LWIT. The support plates in Figure 3a were made of polyether ethyl ketone (PEEK) and were drilled with 24 holes in each plate. The positions of the holes were located according to the simulated results. The height and width are 7.6 mm and 6.7 mm, respectively. The accuracy of the position of each hole is ±0.05 mm, which has a negligible effect on the mass resolution according to the simulation results. The diameter of each hole is 0.23 mm, and the diameter of each stainless steel wire is 0.2 mm. The tension applied on the wires is provided by eight nuts on four threaded rods. The distance between the two plates is 62 mm. The distances between the Y copper shields and X copper shields are 16.8 mm and 14 mm, respectively. A gated electron gun was used for ionizing neutral molecules inside the LWIT. In addition, a magnetic ring was set outside the electron gun and used to confine the trajectory of electrons. The effects of magnetic ring was not evaluated, but it is believed that the ionization efficiency could be improved at least 1 order of magnitude from previous work.[38]

An rf signal (1.53 MHz) was applied to the 12 Y wires. A positive dc voltage of up to 23 V was applied to the end ring electrodes to provide a dc trapping potential well for positive ions along the Z axis. The static potential applied on the filament is −60 V. Trapped ions were mass selectively ejected by scanning the rf amplitude at a rate of 3830 Th/s. An ac signal, generated by an arbitrary waveform generator (SRS DS345, Stanford Research Systems, Sunnyvale, CA) was applied on the left six X wires to provide the quasi-dipolar field that facilitated ion ejection during the rf scan. The ions ejected from the LWIT were detected using an electron multiplier, operated at −1400 V. The signal was first amplified using a preamplifier (Keithley 427 current amplifier, Beaverton, OR), and then acquired using a digital oscilloscope (Teledyne LeCroy wavesurfer 3024, Chestnut Ridge, NY) at a sampling rate of 500k samples/s.

The vacuum was supported by a turbo pumping station (HiCube, Pfeiffer, Nashua, NH) with a pumping speed of 35 L/s for N_2. Helium was used as the buffer gas at an indicated pressure of 6×10^{-4} mbar, as measured using a Bayert-Alpert-type ionization gauge (FRG-720, Agilent, Santa Clara, CA) without calibration. The headspace vapor of the organic compounds or sample gas was leaked into the vacuum through a leak valve (Granville-Phillips Co., Boulder, CO) to maintain an indicated pressure of 2×10^{-5} mbar.

RESULTS AND DISCUSSION

Stability Diagram. Figure 4 shows the parameters under which ions are stably trapped (stability diagram) in both experiment and simulation, along with fitted lines. The

DOI: 10.1021/acs.analchem.6b01830
Anal. Chem. 2016, 88, 7800−7806

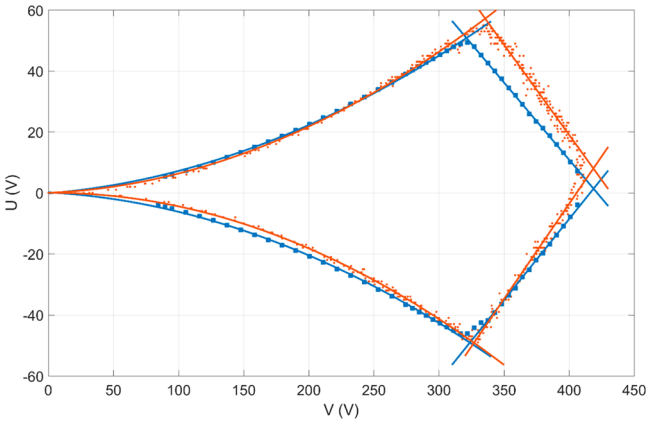

Figure 4. Stability diagram was plotted by monitoring the signal at S/N = 2 of benzene (m/z = 78) at boundary ejection. Small red dots are simulation data; red lines are fitted from the simulation data; blue squares are experimental data; blue lines are fitted from experimental data.

simulation and experimental results fit well in three boundaries (β_x= 1, β_x = 0, and β_y = 0). The simulation boundary of β_y = 1 is shifted to right and top from the experimental results. The ion ejection direction indicated in Figure 2b,d can be understood in terms of this stability diagram. As the U coordinate for intersection points by the β_x = β_y = 1 stability diagram boundaries in both experiment and simulation are higher than 0, ions are more stable in the Y direction than the X direction when they reach the stability boundary along a working line of U = 0.

Comparison of Simulation and Experimental Results under Boundary Ejection. As indicated in the stability diagram and Figure 2b,d, in the current setup, most ions are ejected in the X direction. To verify that, we compared the mass spectra from experiment and simulation. Figure 5 shows good agreement of both resolution and ion ejection direction in mass spectra obtained from simulation and experiment using boundary ejection. The simulated peak at m/z = 98 fits well with the experiment. Because the simulated peak at m/z = 91/92 is formed by ions at m/z = 91, the overlap of m/z = 91 and

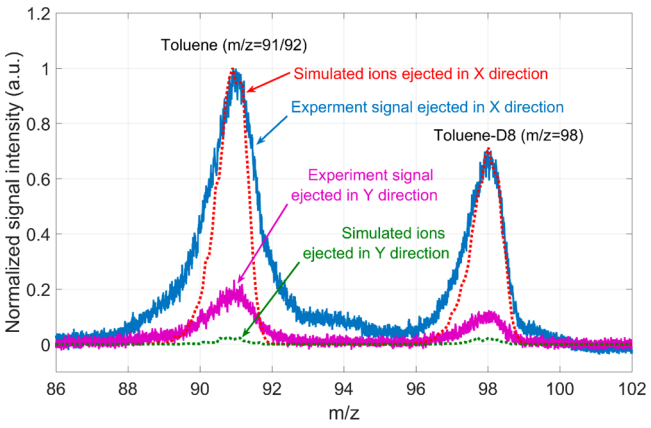

Figure 5. Comparison between experimental and simulated mass spectra using boundary ejection. The sample compounds are toluene and deuterated toluene (toluene-D8). Experimental mass spectra are normalized according to the strongest peak, and two peaks in the simulation mass spectra are normalized according to the relative peak intensities from the experiment.

92 in experimental mass spectrum results in a wider peak than simulated. For the ion ejection direction, experimental results show that more ions are ejected in the X direction (blue solid line vs purple solid line), which was consistent with the simulation results (red dotted line vs green dotted line). The differences of peak intensity between experiment and simulation are also visible in the mass spectra in the Y direction. The signal in the Y direction in the experiment is higher than that in simulations. This can be explained by the β_x = β_y = 1 intersection points in the stability diagram. The intersection points in simulation (U = 8 V) are higher than that in experiment (U = 1.36 V), indicating that the ions are more easily ejected in the X direction in the simulation than in the experiment. It may be that the constructed trap is more symmetrical in X/Y than expected or than what was used in the simulations, perhaps due to an unknown issue in mechanical assembly.

Mass Resolution. The mass resolution was evaluated by a mixture of toluene and deuterated toluene (toluene-D8) with a ratio close to 1:1. Figure 6 shows the mass spectrum for the

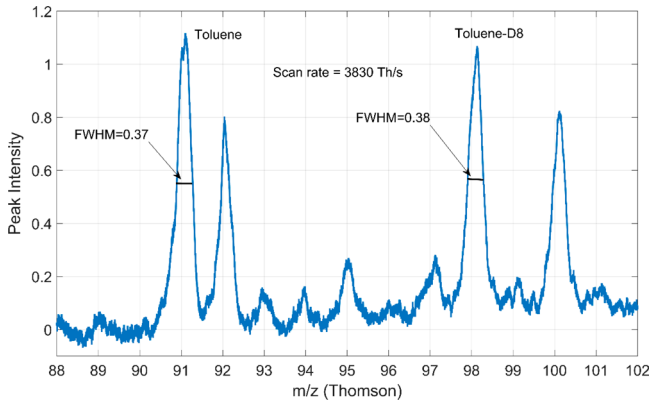

Figure 6. Mass spectrum of a mixture of toluene and deuterated toluene (toluene-D8).

mixture averaged over 50 scans. The fwhm values of major peaks are in the range of 0.37 to 0.38 Th under scan rate of 3830 Th/s. The rf frequency is 1.53 MHz, with applied supplementary ac at frequency of 525 kHz, amplitude of 1.2 V (0-p), and offset of 1.3 V. Ions are resonantly ejected at q = 0.78.

Sample Test. A mixture of 1,2-dichlorobenzene (DCB) and tetrabromoethane (TBE) was introduced into the chamber through the leak valve. Figure 7 shows the mass spectrum of the mixture averaged over 50 scans. The molecular ions of DCB and fragments of TBE were detected. The molecular ions of TBE (345 Th) exceed our current mass range. The mass range under our current rf power supply is from 54 to 210 Th, which agrees with our prediction in simulation (Table 1).

Limits of Detection (LODs). Instrument sensitivity was studied using mixed gas samples of benzene and toluene, both at concentrations of 10 ppmv. In the sample preparation, benzene and toluene were injected using a 5 μL syringe into a 6 L sample bag filled with pure nitrogen. After 3 h, the sample gas mixture was introduced into the mass spectrometer through a leak valve. The sample pressure was kept at around 4 × 10^{-5} mbar, and the working pressure was 6 × 10^{-4} mbar. The mass spectrum was acquired using the detector in the X direction, and the signal was averaged over 50 mass scans. Figure 8 shows the resulting signal, indicating the peaks used for calculating the

DOI: 10.1021/acs.analchem.6b01830
Anal. Chem. 2016, 88, 7800−7806

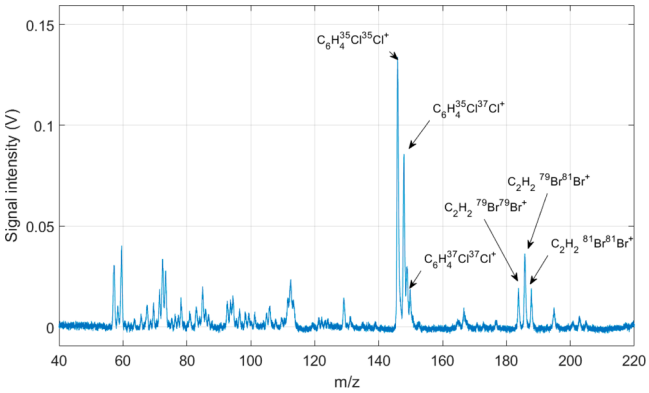

Figure 7. Mass spectrum of a mixture of 1,2-dichlorobenzene and tetrabromoethane.

S/N. The estimated LODs for benzene and toluene are 137 ppbv and 401 ppbv, respectively.

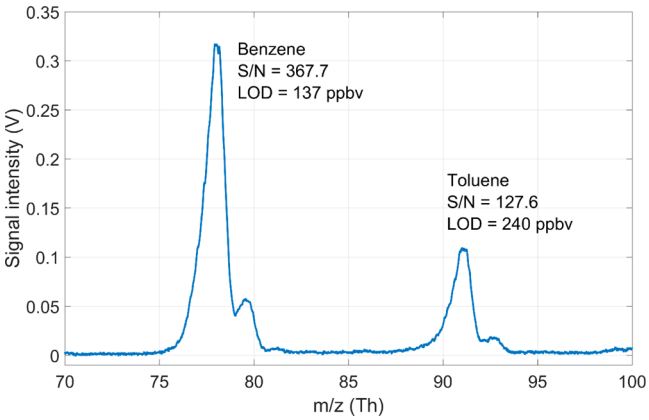

Figure 8. Mass spectrum for mixture sample of benzene and toluene at concentration of 10 ppmv. The LODs were calculated based on S/N = 3.

The good sensitivity of the LWIT can be attributed to two features. First, the designed LWIT primarily ejects ions in the *X* direction. Second, the ion transmission through wires is high, which improves the detection efficiency and increases the sensitivity. The simulated transmission rates are 77% and 69% for ions detected in the *X* direction and the *Y* direction, respectively.

Other Properties. As wires have less surface area, the capacitance in such structure should be much lower than that in solid metal electrodes. The measured capacitance from half-scaled LWIT is 7 to 9 pF, whereas the capacitance in normal LIT with solid metal electrode is higher than 20 pF. Lower capacitance reduces the load for an rf power supply and thus is helpful for saving power and reducing the weight and size of the power supply. The other benefit from using wires is reduced weight. Our half-size LWIT has a total weight of 24 g, which is much lighter than an LIT with a similar size. No effort was made in this study to reduce the weight of the grounded shielding, which was 244 g in this design. This could be significantly reduced if replaced with thinner material or with metal grids. Both of the above features are desirable for a portable device.

The LWIT has relatively high tolerance to the mechanical and assembly error. The simulation shows that the error of the hole position at ±0.1 mm has little impact on the resolution in the half-sized LWIT, whereas the mechanical error can be controlled to within ±0.05 mm. The two supporting plastic plates have five potential misalignments (*X*, *Y*, pitch, yaw, and roll), all of which reduce the distances between wires. Because all the wires are parallel and the distance between the two plates is much larger than the distance between wires, the misalignment of these five misalignments have negligible impact on the geometry. For example, the misalignment of *X* or *Y* misalignment of 1 mm causes 0.00013 mm distance reduction between wires, and one degree of misalignment of roll (twisting or torsion) causes 0.000007 mm distance reduction between wires. The tension applied on the wires can cause a distortion on the two end plates. This distortion is reduced by adding a metal shim in the next generation of LWIT. However, this distortion also has little impact on the geometry of the LWIT. For example, one degree of such distortion causes 0.0012 mm distance reduction between top and bottom wires.

One other distinguishing feature of the WIT is that photons can go through the ion trap in any direction. The calculated transmission for photons are 76.3% and 71.4% from the *X* and the *Y* directions, respectively. This feature is especially suitable for photon dissociation in an MS/MS experiment.

CONCLUSIONS

A LIT made of 24 wires supported between two insulator plates has been studied in simulation and then evaluated experimentally. The electric field distribution inside the LWIT is very similar to that in the conventional LIT with hyperbolic-curved electrodes. The geometry for the LWIT was optimized using a two-parameter approach based on the criteria of resolution and peak intensity. Employing an optimized geometry, a test system was built to evaluate the performance of the LWIT. The experimental results agree well with the simulation results as presented in the stability diagram, the ion ejection direction, and resolution under boundary ejection. Under normal working conditions, the fwhm was found to be in the range of 0.37−0.38 Th for a scan rate of 3830 Th/s. The LODs were 137 ppbv and 401 ppbv for benzene and toluene, respectively. The LWIT exhibits high ion and photon transmission, low capacitance, high tolerance to mechanical and assembly error, and low weight, which could benefit the development of a miniaturized LIT system.

ASSOCIATED CONTENT

Supporting Information

The Supporting Information is available free of charge on the ACS Publications website at DOI: 10.1021/acs.analchem.6b01830.

Isopotential curves in a hyperbolic-electrode LIT and impact of ground electrodes to the resolution and detected ions (PDF)

AUTHOR INFORMATION

Corresponding Author

*E-mail: austin@chem.byu.edu.

Notes

The authors declare no competing financial interest.

ACKNOWLEDGMENTS

Work at Brigham Young University was funded by the National Science Foundation (United States) Chemical Measurement

DOI: 10.1021/acs.analchem.6b01830
Anal. Chem. 2016, 88, 7800−7806

and Imaging Program and at Stanford University by the U.S. Air Force Office of Scientific Research.

REFERENCES

(1) Zhou, M.; Morgner, N.; Barrera, N. P.; Politis, A.; Isaacson, S. C.; Matak-Vinkovic, D.; Murata, T.; Bernal, R. A.; Stock, D.; Robinson, C. V. *Science* **2011**, *334*, 380−385.
(2) Cravatt, B. F.; Simon, G. M.; Yates, J. R., III *Nature* **2007**, *450*, 991−1000.
(3) Aebersold, R.; Mann, M. *Nature* **2003**, *422*, 198−207.
(4) Ong, S. E.; Mann, M. *Nat. Chem. Biol.* **2005**, *1*, 252−262.
(5) Domon, B.; Aebersold, R. *Science* **2006**, *312*, 212−217.
(6) Badman, E. R.; Cooks, R. G. *J. Mass Spectrom.* **2000**, *35*, 659−671.
(7) Berchtold, C.; Bosilkovska, M.; Daali, Y.; Walder, B.; Zenobi, R. *Mass Spectrom. Rev.* **2014**, *33*, 394−413.
(8) Jarmusch, A. K.; Cooks, R. G. *Nat. Prod. Rep.* **2014**, *31*, 730−738.
(9) Kogan, V. T.; Lebedev, D. S.; Pavlov, A. K.; Chichagov, Y. V.; Antonov, A. S. *Instrum. Exp. Tech.* **2011**, *54*, 390−396.
(10) Sanders, N. L.; Sokol, E.; Perry, R. H.; Huang, G. M.; Noll, R. J.; Duncan, J. S.; Cooks, R. G. *Eur. Mass Spectrom.* **2010**, *16*, 11−20.
(11) Scherl, A. *Methods* **2015**, *81*, 3−14.
(12) Snyder, D. T.; Pulliam, C. J.; Ouyang, Z.; Cooks, R. G. *Anal. Chem.* **2016**, *88*, 2−29.
(13) Schwartz, J. C.; Senko, M. W.; Syka, J. E. P. *J. Am. Soc. Mass Spectrom.* **2002**, *13*, 659−669.
(14) Ouyang, Z.; Wu, G. X.; Song, Y. S.; Li, H. Y.; Plass, W. R.; Cooks, R. G. *Anal. Chem.* **2004**, *76*, 4595−4605.
(15) Gao, L.; Song, Q. Y.; Patterson, G. E.; Cooks, R. G.; Ouyang, Z. *Anal. Chem.* **2006**, *78*, 5994−6002.
(16) Keil, A.; Hernandez-Soto, H.; Noll, R. J.; Fico, M.; Gao, L.; Ouyang, Z.; Cooks, R. G. *Anal. Chem.* **2008**, *80*, 734−741.
(17) Gao, L.; Cooks, R. G.; Ouyang, Z. *Anal. Chem.* **2008**, *80*, 4026−4032.
(18) Ouyang, Z.; Noll, R. J.; Cooks, R. G. *Anal. Chem.* **2009**, *81*, 2421−2425.
(19) Fico, M.; Yu, M.; Ouyang, Z.; Cooks, R. G.; Chappell, W. J. *Anal. Chem.* **2007**, *79*, 8076−8082.
(20) Xiao, Y.; Ding, Z. Z.; Xu, C. S.; Dai, X. H.; Fang, X.; Ding, C. F. *Anal. Chem.* **2014**, *86*, 5733−5739.
(21) Sudakov, M. Y.; Apatskaya, M. V.; Vitukhin, V. V.; Trubitsyn, A. A. *J. Anal. Chem.* **2012**, *67*, 1057−1065.
(22) Li, X. X.; Zhang, X. H.; Yao, R. J.; He, Y.; Zhu, Y. Y.; Qian, J. *J. Am. Soc. Mass Spectrom.* **2015**, *26*, 734−740.
(23) Wang, L.; Xu, F. X.; Dai, X. H.; Fang, X.; Ding, C. F. *J. Am. Soc. Mass Spectrom.* **2014**, *25*, 548−555.
(24) Zhang, Z. Y.; Li, C. P.; Ding, C. F.; Xu, F. X.; Li, B. Q.; Huang, Q. B.; Xia, H. X. *Rapid Commun. Mass Spectrom.* **2014**, *28*, 1764−1768.
(25) Dang, Q. K.; Xu, F. X.; Huang, X. H.; Fang, X.; Wang, R. Z.; Ding, C. F. *J. Mass Spectrom.* **2015**, *50*, 1400−1408.
(26) Li, A. L.; Hansen, B. J.; Powell, A. T.; Hawkins, A. R.; Austin, D. E. *Rapid Commun. Mass Spectrom.* **2014**, *28*, 1338−1344.
(27) Hansen, B. J.; Niemi, R. J.; Hawkins, A. R.; Lammert, S. A.; Austin, D. E. *J. Microelectromech. Syst.* **2013**, *22*, 876−883.
(28) Ray, T.; Jyothi, S.; Ram, N. B.; Rangwala, S. A. *Appl. Phys. B: Lasers Opt.* **2014**, *114*, 267−273.
(29) Pita, J. R. C. *Design, Development and Operation of Novel Ion Trap Geometries*. Ph.D. Dissertation, University of London, London, U.K., 2007.
(30) Wang, Y.; Wanczek, K. P. *J. Chem. Phys.* **1993**, *98*, 2647−2652.
(31) Higgs, J. M.; Austin, D. E. *Int. J. Mass Spectrom.* **2014**, *363*, 40−51.
(32) Sudakov, M. *Int. J. Mass Spectrom.* **2001**, *206*, 27−43.
(33) Wu, G. X.; Cooks, R. G.; Ouyang, Z. *Int. J. Mass Spectrom.* **2005**, *241*, 119−132.
(34) Zhang, Z. P.; Quist, H.; Peng, Y.; Hansen, B. J.; Wang, J. T.; Hawkins, A. R.; Austin, D. E. *Int. J. Mass Spectrom.* **2011**, *299*, 151−157.
(35) Xiong, X.; Xu, W.; Fang, X.; Deng, Y.; Ouyang, Z. *J. Am. Soc. Mass Spectrom.* **2012**, *23*, 1799−1807.
(36) Remes, P. M.; Syka, J. E. P.; Kovtoun, V. V.; Schwartz, J. C. *Int. J. Mass Spectrom.* **2014**, *370*, 44−57.
(37) Wu, Q.; Tian, Y.; Li, A.; Austin, D. E. *Int. J. Mass Spectrom.* **2015**, *393*, 52−57.
(38) Wu, Q.; Hua, L.; Hou, K.; Cui, H.; Chen, W.; Chen, P.; Wang, W.; Li, J.; Li, H. *Anal. Chem.* **2011**, *83*, 8992−8998.

DOI: 10.1021/acs.analchem.6b01830
Anal. Chem. 2016, 88, 7800−7806